


Article

Nearshore Sandbar Classification of Sabaudia (Italy) with LiDAR Data: The FHyl Approach

Andrea Taramelli ^{1,2} , Sergio Cappucci ^{3,*}, Emiliana Valentini ¹, Lorenzo Rossi ¹ and Iolanda Lisi ¹

¹ Institute for Environmental Protection and Research (ISPRA), via Vitaliano Brancati 48, 00144 Rome, Italy; andrea.taramelli@isprambiente.it (A.T.); emiliana.valentini@isprambiente.it (E.V.); lorenzo.rossi@isprambiente.it (L.R.); iolanda.lisi@isprambiente.it (I.L.)

² Istituto Universitario di Studi Superiori di Pavia (IUSS), Piazza della Vittoria 15, 27100 Pavia, Italy

³ National Agency for new technologies energy and sustainable development (ENEA), via Anguillarese 301, 00123 Rome, Italy

* Correspondence: sergio.cappucci@enea.it; Tel.: +39-063-048-3415

Received: 14 February 2020; Accepted: 18 March 2020; Published: 25 March 2020



Abstract: An application of the FHyl (field spectral libraries, airborne hyperspectral images and topographic LiDAR) method is presented. It is aimed to map and classify bedforms in submerged beach systems and has been applied to Sabaudia coast (Tirrenyan Sea, Central Italy). The FHyl method allows the integration of geomorphological observations into detailed maps by the multisensory data fusion process from hyperspectral, LiDAR, and in-situ radiometric data. The analysis of the sandy beach classification provides an identification of the variable bedforms by using LiDAR bathymetric Digital Surface Model (DSM) and Bathymetric Position Index (BPI) along the coastal stretch. The nearshore sand bars classification and analysis of the bed form parameters (e.g., depth, slope and convexity/concavity properties) provide excellent results in very shallow waters zones. Thanks to well-established LiDAR and spectroscopic techniques developed under the FHyl approach, remote sensing has the potential to deliver significant quantitative products in coastal areas. The developed method has become the standard for the systematic definition of the operational coastal airborne dataset that must be provided by coastal operational services as input to national downstream services. The methodology is also driving the harmonization procedure of coastal morphological dataset definition at the national scale and results have been used by the authorities to adopt a novel beach management technique.

Keywords: FHyl; sand bar; bedform classification; beach; morphology; LiDAR; DSM

1. Introduction

Nearshore bar dynamics are the main expression of breaking-wave-induced hydrodynamics and sediment transport patterns taking place along the coast. Morphological changes with respect to the equilibrium beach profile features (e.g., number, shape, location and configuration of nearshore bars and troughs, the distance of outer and inner bar crest from the shoreline, etc.) are an important topic of coastal research [1,2], as they provide basic information on sedimentary processes under different wave climate. Therefore, the detection of multiple beach profiles is relevant to a proper coastal management and it is often required to implement effective beach erosion control also using mathematical models to simulate deterministic scenarios.

When beach morphology changes, the use of morphodynamic classification of the beach system is often recommended [3,4]. It should be based on the analysis of coastal processes and beach response under a wide range of physical parameters. In this regard, the dimensionless sediment fall velocity

(often referred to as the Dean number) and the wave steepness are commonly considered as key parameters to predict and define the nature (barred or non-barred) of a cross-shore equilibrium profile (e.g., [5]). Past researches have proposed several methods to predict the nature of the cross-shore equilibrium profile and to classify the beach morphodynamic state based on the detection of different bars systems in the surf zone [1,6]. The most recent and complete classifications take into account the interaction between the main physical parameters (i.e., wave energy, sediment grain size, seabed slope, shape of bed forms, etc) that affect the equilibrium of both the cross-shore and alongshore beach profile (e.g., [7–9]).

However, morphological changes on barred beaches profile are required as they cover a wide range of spatial and temporal scales. Stive et al. [3] refer to the middle-term time scale (i.e., inter-annual and inter-decadal variability) in the cases of surf zone bar cycles and of wave climate variations, while refer to the short-term time scale (i.e., from inter-seasonal to hours variability) to assess periodic fluctuations ranging from single to seasonal events (e.g., one or few tidal cycles and wave conditions, high-energy or storm surge events) driven by breaking waves.

Traditional topo-bathymetric in situ measurements (i.e., total station/GPS and echo-sounder) cannot address this wide range of scales, because of the practical difficulties to detect the nearshore bedform's variability which make these survey time consuming and very expensive. Instead, remote sensing data (e.g., SAR, optical images and LiDAR data) provide accurate topographic and bathymetric data sets with a spatial resolution large enough to cover a relatively wide area, including the submerged beach profile, with a uniform temporal resolution alongshore [10–14].

The research development for studying coastal environments, characterized by high spatial and temporal variability, is very promising as it is based on integrated tools that allow: 1) to analyze the different morphological components with high quality standards for ensuring a realistic and accurate order; and 2) to detect (and minimize) undesired changes at early stages.

In this context the airborne LiDAR (light detection and ranging) technology is considered a very powerful tool for beach monitoring and investigation, since it allows collecting data over a short time frame, providing a full overview at a larger scale with good spatial and vertical accuracy [15,16]. The LiDAR technology is a respectable support tool for the morphological characterization in shallow water (less than 1 m depth; [17–19]). LiDAR system is a scanner that deflects a laser beam across the flight line and detects its reflection, so that a swath of ground along the flight line is sampled point wise. The production of a DSM (digital surface model) and DTM (digital terrain model) on a wide scale range, regardless of the site characteristics, shows that laser altimetry technology is spreading through the use of LiDAR bathymetric airborne [16–19].

Numerous examples of coastal monitoring studies focused on the integration of field- and remote sensing- data may be cited [20–26]. Besides morphometric analysis, other approaches, based on the use of Geomatics techniques, can provide important support for the study of vulnerability status of coastal systems [27–29]. Multispectral and hyperspectral remote sensing provide data sets that allow to map the seabed and habitat heterogeneity [30,31], to study the cover of vegetation in wetlands [32,33] and to map plant species in submerged shallow water areas [34–38].

The research activities we carried out in the last ten years, in a synergic way with coastal end-users, EO experts and coastal processes experts, allowed the development of the innovative FHyL (field spectral libraries, airborne hyperspectral images and topographic LiDAR) approach. The FHyL method supports the collection and analysis of remote sensing operational dataset for coastal applications and management; in particular, it lets integration of different geomorphological observations into detailed maps by the multisensory data fusion process from LiDAR and hyperspectral data [31].

The aim of the present work is to provide and make available to the wider public a series of calibrated and validated data and products, usable as the benchmark for National LiDAR acquisition [39]. In particular, an application of the FHyL approach to the Sabaudia (Tirrenyan Sea, Italy) case study is herein described. This application has provided a subdivision of the coast into different zones, starting from the analysis and the classification of the main morphological features detected in the nearshore.

However, due to the absence of vegetation on the seafloor, hyperspectral data have not been included in the present research, but have rather been used on other case studies and applications as part of the FHyL [31]. Despite this, the analysis of nearshore bathymetry allowed to identify the main submerged beach features affecting the coastal evolution and to characterize their key morphological parameters (e.g., slope and direction of bed-forms, grain size, and water depth).

This work also provides a series of services for coastal mapping aimed to make available the products obtained by the processing of remote sensing data for research purposes and thus, to bridge the gap between scientific community and different technical experts and stakeholders.

2. Study Area

Sabaudia beach is a sandy coastal stretch of about 35 km length located in the Lazio Region (Tyrrhenian Sea, central Italy) between the Torre Astura and the San Felice Circeo Promontory (Figure 1) and oriented in a NW-SE direction.

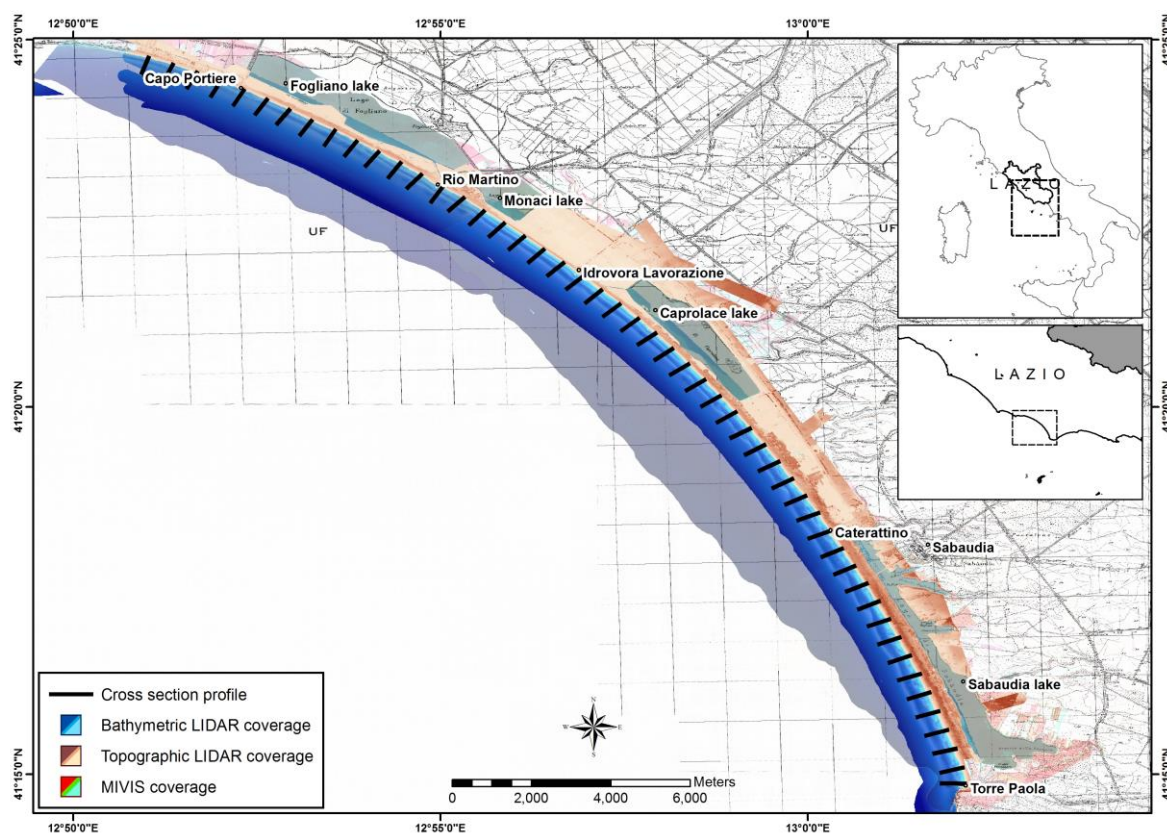


Figure 1. Sabaudia study area along the Lazio Region (Tyrrhenian Sea, Italy). The figure shows: Topographic and Bathymetric LiDAR data, MIVIS coverage and cross section profiles (500 m spaced) used for the analysis.

This coastal area is characterized by the presence of relevant economic and touristic activities and several environmental sensitive habitats and species (both flora and fauna). The morphological and ecological features reflect the extreme lively dynamics of emerged and submerged beach, resulting in macro and micro changes of the equilibrium profile [19,40].

The emerged beach is limited by an almost uninterrupted coastal dune that mainly follows the shoreline direction [41] (Figure 2). The coastal dunes formation has been related to sandy bar systems due to the increased sea level rise during the Versilian's age [42,43]. Shoreline and dune foot are influenced by the wind regime and, more precisely, periodically undulated in shape under the effect of both NW and SW winds. Coastal dunes tend to increase in term of proportion and amplitude moving towards the N-S direction, reaching the highest elevation of about 28 m (including vegetation)

and width of about 250 m [19,42]. Dune formations are established by root systems of the typical Mediterranean coastal vegetation providing the dynamic stability and positive feedback between the vegetation and sediments [40,43,44]. The free morphological exchange between coastal dunes and submerged sandy bar systems has been prevented by the construction of the coastal road, in the 1950s, along the longitudinal axis of dune crest. In order to mitigate the induce runoff processes and to preserve the beach-dune system, the stretch of the road between the Rio Martino mouth and Idrovora di Lavorazione has been successively removed (in the 1980s).



A - Vegetation cover of foredune



B – Un-vegetated foredune



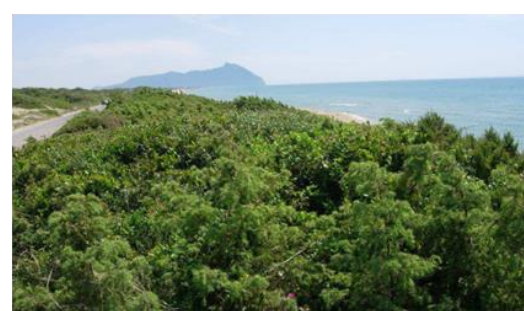
C – Emerged beach



D – Blowout



E – Walkway and blowout



F – Vegetated dune crest
(Circeo in background)

Figure 2. Pictures of different parts of the study area. (A) Vegetation cover of foredune; (B) Un-vegetated foredune; (C) Emerged beach; (D) Blowout; (E) Walkway and blowout; (F) Vegetated dune crest (Circeo in background).

It is a microtidal environment and the influence of tidal currents within the studied area can be considered negligible as tidal range varies between 0.15 and 0.45 cm (www.mareografico.it). Wave climate indicates that it is a fetch-limited site with low wave energy. Wave height (H_s), mainly varying from 0.5 to 1 m, suggests a predominance of waves coming from West direction (www.idromare.it). The high energy waves (storms conditions) prevalently occur in the central part of the study site,

where most evident flooding and erosion phenomena (sometimes reaching the foot of the dune and the coastal road) are highlighted [40].

The submerged beach is characterized by a very mild slope profile with a mean sediment diameter of about 0.01 mm (maximum value of about 0.035 mm is reached near the rocky coast of the S. Felice Circeo Promontory). The sand collected within the active beach is characterized by a median diameter (D_{50}) between 0.14 and 0.24 mm [40,44]. The sandy bar system is mainly located within the -5 m depth from the shoreline, while there are no significant changes in the submerged beach slope up to -10 m depth. Rhythmic shoreline features appear along with a series of bars and strong nearshore circulation suggesting the presence and formation of rip-current [40]. The morphology of the submerged beach was not known before the present study, and here we discuss how it varies from North to South as the northerly part is suffering from coastal erosion. Net longshore transport is directed from North to South. It is higher in the northern part (up to $20,000$ m³/y in front of Fogliano coastal Lake) and lower in the southern part (less than $10,000$ m³/y in front of Sabaudia coastal Lake) [44].

3. Materials and Methods

3.1. Materials

LiDAR survey for collecting elevation data both in emerged and submerged environment was conducted on 9th May 2009 during good weather conditions. Dataset (~ 24 km²; 6×10^6 pts) was used to interpret features in shallow waters that in the study area were observed for the first time ever on upper shoreface thanks to data acquisition and elaboration discussed in the present study. The objective of this study was achieved using the bathymetric LiDAR sensor Hawk eye II dataset [45,46] provided by the BLOM-CGR©.

The bathymetric LiDAR uses radiations in infrared band (wavelength of 1064 nm), for the free surface acquisitions, and in the green band (wavelength at 532 nm) for the seabed acquisitions [46]. With 42 strips for the Sabaudia area, the cover extended up to -26 m depth. The depths identified by bathymetric LiDAR were detected for each pulse from the time differences between the feedback signal received from the water surface and the return signal received from the seabed [47]. The effects of surface waves [48] and errors of measurement on the surface [49] were eliminated by using the methodology suggested by [50]. Bathymetric point density was maintained at about 1 point for m² and a nominal horizontal and vertical accuracy of ± 0.5 cm and ± 0.15 cm, respectively. Technical characteristics of the LiDAR HawkEye II sensor are reported in Table 1.

Table 1. Main Technical features of bathymetric LiDAR sensor and positioning system.

LiDAR HawkEye II	
Bathymetric LiDAR Frequency	64,000 Hz
Altitude	From 250 to 500 m
Swath	From 100 to 330 m
bathymetric points density	From 0.2 to 0.3 pt/m ²
Accuracy of Topographic survey	Horizontal: ± 0.5 m Vertical: ± 0.15 m

3.2. Field Measurements

An in-situ campaign was also performed before LiDAR acquisition survey, on April 2009, in order to collect bathymetric data using a single beam acoustic sensor FURUNO' FCV-600L (200 khz) along beach profile perpendicular to the shoreline (maximum length 1.5 km). Furthermore, transparency of coastal water was estimated by Bloom during preliminary investigation and expected to be approximately around 12 m (pers. Comm; [51–54]). Therefore, direct measurements of transparency was carried out by using Secchi disk in front of Astura river mouth only, where transparency is lower compared to the southern part of the coastal stretch (result: 4–5 m).

Ten transects, perpendicular to the shoreline, were chosen to detect submerged beach profiles from about 1 m up to 10 m of depth. About 1000 m of survey lines were collected before LiDAR acquisition. All in situ data acquisition was carried out during low wind, calm sea, and vertical sunlight conditions.

3.3. Methodology

In this paper the modular FHyl approach (Figure 3), is implemented for the analysis of submerged coastal areas in order to characterize the spatial scale of sand bar distribution [55]. The flowchart of the adopted methodology is shown in Figure 4.

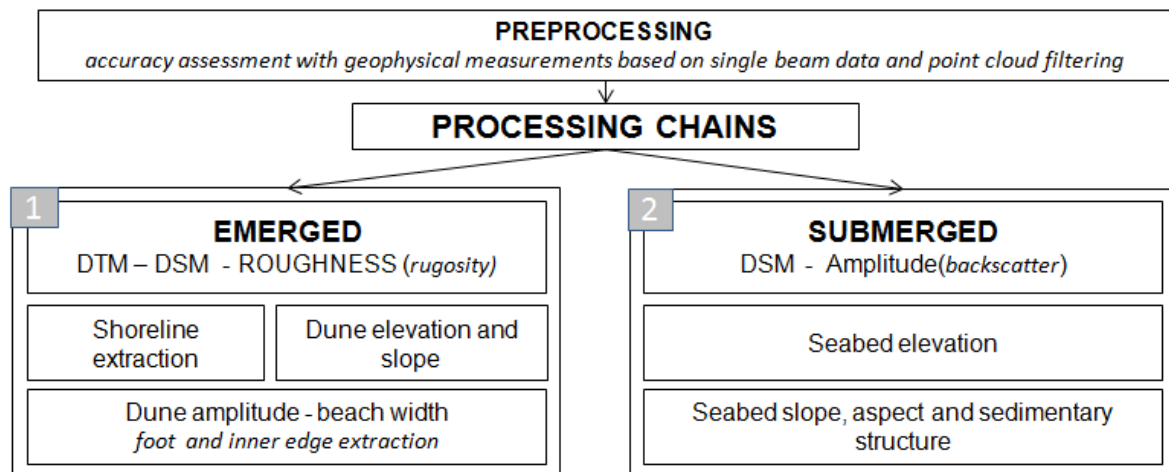


Figure 3. Scheme of the processing chain of the FHyl approach. The module 2 represents the FHyl module to be used for the characterisation of submerged coastal areas (see [51] for more details).

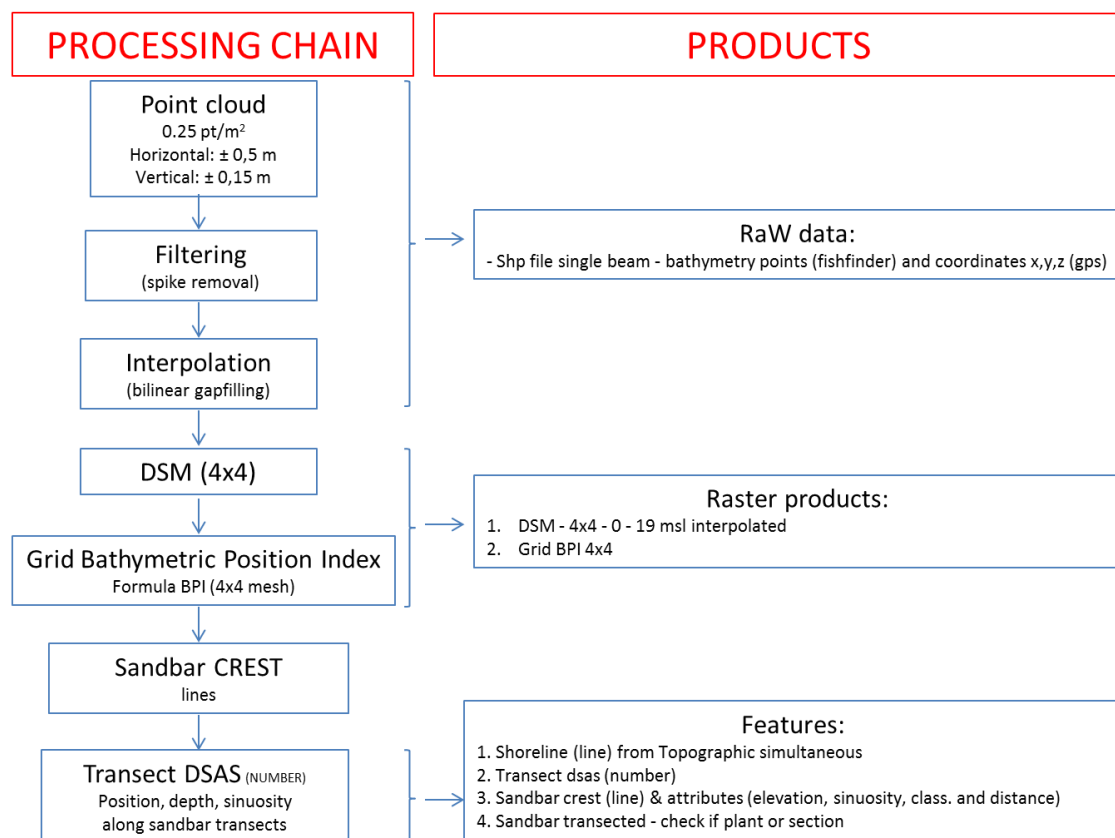


Figure 4. Flowchart of the LiDAR processing chain (left) used in the present work and products (right).

3.3.1. Parameters Extraction from Bathymetric LiDAR Data

Standard deviation of the LiDAR point cloud was calculated on a 4×4 m grid for obtaining an accurate interpretation and classification of: (1) seafloor morphology, (2) rugosity, and (3) consolidated and unconsolidated seabed. By the application of morphometric slope and curvature parameters, complex sedimentary structure of the sand bars were analyzed. The size, orientation, and asymmetry of several bedforms observed in shallow water were described to better understand their formation and evolutionary trend under the effect of longshore currents, incident waves and wind regime.

Then, the analysis of sandy bar distribution along the coastal stretch was enhanced combining specific indexes and parameters, such as sandy bar order, extent and asymmetry.

3.3.2. DSM Generation: Bathymetry

The final point cloud of LiDAR was processed to obtain the topographic and bathymetric DSMs on regular grids. In the present paper we use and discuss only bathymetric dataset. The raw strips, acquired during the overpass, were arranged in parallel and overlap the sides for about 20–30% (Figure 5a). The final point cloud LiDAR (Figure 4b), due to inhomogeneity in the points' density of the surveys [15,49,55–57], were more focused on the edges of the strips.

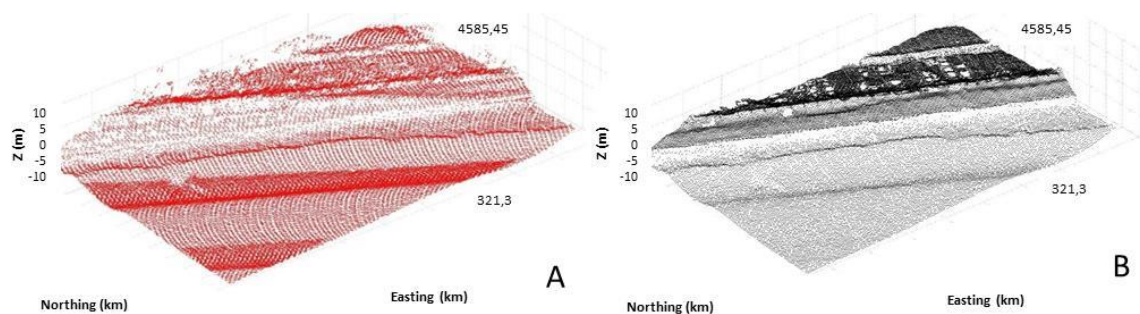


Figure 5. Three-dimensional representation of the different density and spatial distribution obtained for (a) point cloud and (b) final DSM. The comparison shows the greater dispersion of the LiDAR point cloud (presence of abnormal measurements or peak) compared to the final 4×4 DSM.

By using the “import Hawkeye” conversion wizard, the raw data acquired along the flight line (.dat extension) were imported in CARIS Hips and Sips [1] and carefully analysed, for data cleaning (remove spike) and surface processing. Then, according to the density of raw points, a Digital Surface Model (DSM) was obtained by the use of the CARIS[®] software, setting the grid resolution to 2×2 m for the topographic DSM and to 4×4 m for the bathymetric one.

3.3.3. Bathymetric Position Index (BPI)

The bathymetric position index (BPI), representing the marine version of the Topographic Position Index (TPI) introduced by [58], has been applied to several sedimentary [59], geomorphological [60] and seafloor habitat mapping [61] studies. The BPI has been recently used for benthic habitat mapping studies [62–66].

The index, calculated using the Wilson et al. (2007) formula in each raster cell [67], can help in the recognition of the shapes on the seabed. The BPI has been calculated in ArcGis[®] by the Raster Calculator tool as follows:

$$BPI = Z_{grid} - FocalStatistic(Z_{grid}, NbrCircle(r, MAP), MEAN, DATA)$$

where Z_{grid} , $NbrCircle(r, MAP)$, and $MEAN$ are the ArcGis[®] classes, parameters, and variables, r (set to 20 m) is the radius in MAP units of the circular neighbourhood, and the $MEAN [i1] <>$ is processed by the focal-statistic function.

3.3.4. Bars Extraction and Sinuosity

The FileGeoDataBaseRaster (FGDBR) has been imported in ArcGis® as a floating point and masked to remove the inland water (lagoon and coastal lake that are behind the dunes). The shoreline has been extracted from the topographic digital terrain model (DTM; [40]), and the Digital Shoreline Analysis System (DSAS® of USGS; [2]) software was used to trace perpendicular transect with an offset of 500 m (following the methods of [40,44]). The “construct points” editing tool was used to create a dataset of points placed along the transects every 4 m (same spacing of DTM dataset) and then, ArcGis Spatial Analyst Tool “Extract value to point” was applied to the DSM bathymetric values to determine the relative depth values on the transect. The Bathymetric Position Index (BPI) map were used to trace the crest bars every 20 m, as a clipping mask to detect the “upper” areas of the bathymetry by using the following function:

$$\text{Con}(\text{"Bathymetry_4X4_Masked"} == \text{FocalStatistics}(\text{"Bathymetry_4X4_Masked"}, \text{NbrCircle}(5, \text{"CELL"}), \text{"MAXIMUM"})), 1, 0)$$

The function is able to check if a 4×4 m cell (of 16 m^2) is the higher in a circular neighbourhood of 5 cells (covering a total surface of 400 m^2). The crest lines were digitized by using both the information provided by BPI and higher point.

The morphological characterization of sand dunes was based on the calculation of the crest sinuosity, considering that the sinuosity is a geometric properties influenced by substrate and hydrodynamic conditions. More specifically, the crest line sinuosity was extracted from the LiDAR DSM [68,69] and the extracted pixel values were used to obtain a binary image of the sinuosity line. Then, the sinuosity network extraction was performed applying the skeletonization algorithm on the reclassified image. Finally, the degree of the crest sinuosity (S) was quantitatively estimated by using the following relation:

$$S = l/L$$

where l (in m) is the along-line length calculated for each skeletonized branch, while L (in m) is the straight-line distance between the starting and ending points of the observed crest line (the two nodes of each channel network) calculated using Pythagoras' theorem.

4. Results

Many results were obtained by RS processing described above. Longshore Bar-Trough (LBT), Rhythmic Bar and Beach (RBB), Transverse Bar and Rip (TBR), Low Tide Terrace (LTT), and the different barred beaches recognized within the studied area included the Intermediate Barred Beach (IBB) and the Dissipative Barred Beach (DBB). The analysis discussion of morphological characterization is exposed proceeding from NW to SE. Results related to bed forms observation are presented after a brief discussion on the accuracy of the bathymetry measured in the nearshore by using acoustic and remote sensing techniques. Among the obtained results, the following products are provided and made available to a wider public:

RaW data:

1. Shp file single beam – bathymetry points (fishfinder) and coordinates x,y,z (gps)

Raster products:

2. DSM – $4 \times 4 - 0 - 19$ msl interpolated
3. Grid BPI 4×4

Features:

4. Shoreline (from LiDAR)
5. Transect DSAS

6. Sandbar crest (line; number 75)

Attributes elevation and sinuosity and classification and distance:

7. Sandbar parameters (excel file)
8. Transect parameters (excel file)

4.1. Results from LiDAR Survey and Accuracy

The DSM was obtained by creating over a total area of about 24 km² (excluding Circeo Promontory). Its extension varies from the shoreline down to −13 m of depth (reaching the outstanding value of −25 m in the southern part close to the Circeo Promontory/Torre Paola). Then, a shading and lighting relief were applied to highlight the morphology of the DEM area. Finally, for spots of particular interest, specific maps of slope and exposure were created for a better description of features and seafloor morphology.

The accuracy of the submerged LiDAR acquisition was evaluated by the comparison between LiDAR and Single Beam bathymetric data (Figure 6). In particular, traditional assessments accuracy metrics such as the differences in elevation [21–24] were performed. The same spatial resolution was obtained from the measurements acquired by the two bathymetric acquisition systems and used to determine the differences between single-beam and LiDAR acquisitions. The scatter plots of the difference between the two interpolated DSM are reported in Figure 5. The results show a limited but constant overestimation of the LiDAR DSM over the single-beam DSM of about −20 cm. This overestimation slightly increases offshore above 7.5–8 m of depth.

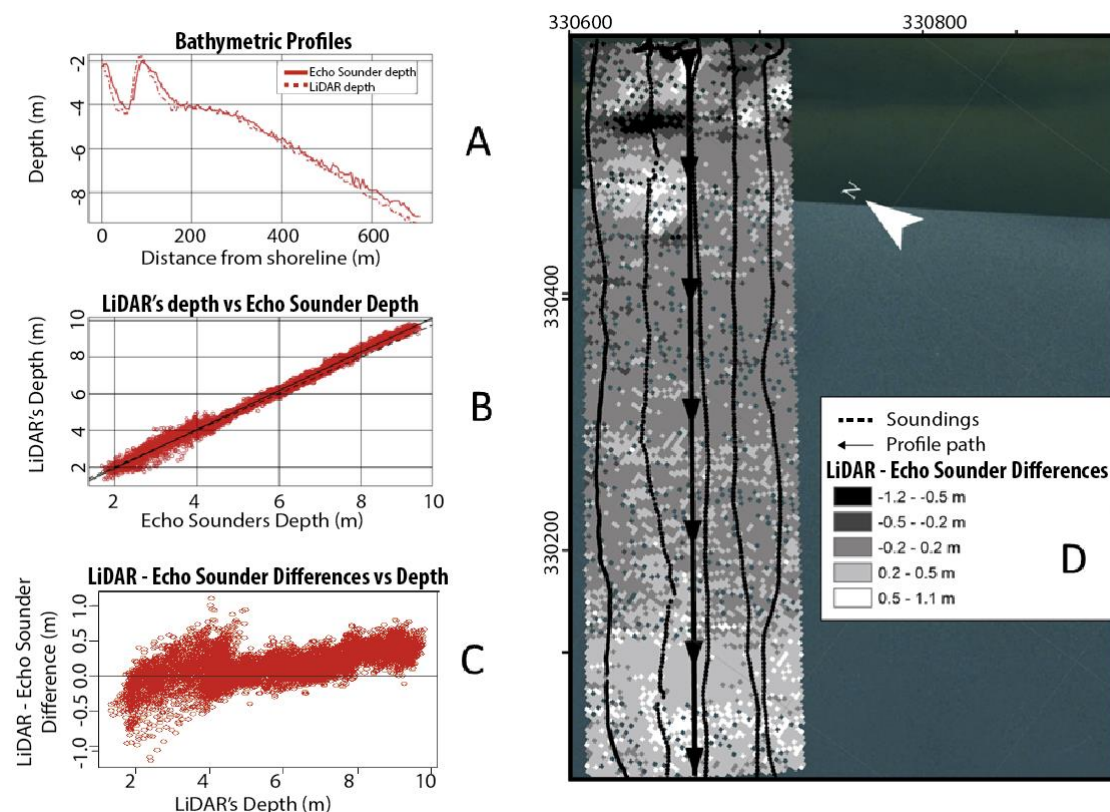


Figure 6. Performance and accuracy of the submerged LiDAR data compared with the single-beam acquisition (A) (top left). The comparison was carried out through a traditional assessments accuracy metrics, such as the differences. (B) (middle left) and (C) (bottom left) show, both the spatial resolution of the different measuring points of the seafloor (determined by differences in the acquisition system with single-beam and bathymetric LiDAR) and the scatter plot of the difference between the two interpolated DSM (D; right).

4.2. Bathymetric Position Index (BPI)

The BPI defines the elevation of locations with reference to the overall landscape. It can be considered as a second order derivative of the DSM as it gave evidence of morphological features like depressions, crest lines and flat areas. Thanks to the map generated by BPI, a bars system can be easily observed (Figure 7).

In the northern part, the presence of the two main crests running parallel to the shoreline can be observed (Figure 7A). Moving southern, the behaviour of the “double bar” system becomes more complex in terms of crest line continuity and shapes (Figure 7B). Here, the two crests have higher sinuosity and the presence of depressions and slope variations indicates the change of the system morphodynamic. The crestline closer to the shoreline loses its continuity and shows a higher sinuosity, while the farthest crest, shows a higher distance from the shoreline and appears slightly undulated (Figure 7C). In the southern part of the study area, a series of small regular cross-shore structures, perpendicular to the shoreline and confined between the two major ridge/bar system, is also evident (Figure 7D).

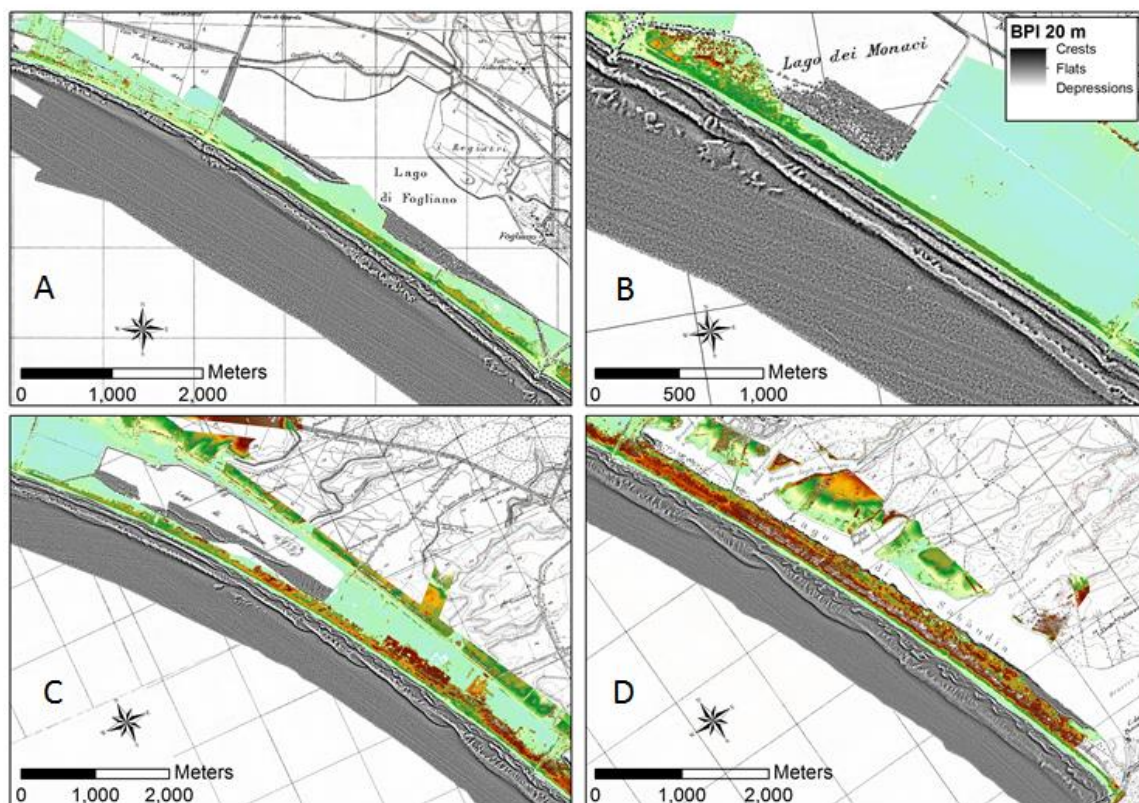


Figure 7. Bathymetric Position Index calculated from DSM. Four examples of bedforms are visualized from North to South: (A) two main crests running parallel to the shoreline; (B) the two crests in (A) become more complex; (C) the crest closer to the shoreline shows a higher sinuosity, while the farthest shows a higher distance from the shoreline; (D) series of small regular cross-shore structures, perpendicular to the shoreline. Note the increasing distance of the bar crests from the shoreline moving southward.

4.3. Submerged Bed Forms Observed in the Nearshore Zone

A great variety of nearshore bedforms are observed by DSM (Figure 8). They have a shape rather flat and asymmetrical in section, mainly caused by the breaking-waves action [70]. The most common morphologies are Longshore Bar and Trough (LBT). By a more accurate analysis of bedforms distribution, the following typologies have been identified.

Inner Bar (IB) and Outer Bar (OB) with some evidence of Long Tide Terrace (LTT) in the southern part are observed in front of the southern part of Fogliano Lake (Figure 8A). In front of Monaci Lake (Figure 8B) a well-developed and linear LTT, IB and OB system is constantly detected. In front of Caprolace Lake (Figure 8C), the OB is still present but the LTT and IB system gradually develop into a Transverse Bar and Rip (TBR) bedform (Figure 8D). A fully developed TBR in the inner part of the submerged beach and an OB system is revealed; a wide shore parallel trough distinguishes this system and a shore-parallel bar interrupted from crescentic bars (which suggests the formation of rip currents; Figure 8E).

Moving southward, near the Circeo Promontory, the transverse bar and rip (TBR; Figure 8F) and Rhythmic Bar and Beach (RBB) are commonly observed closer to the coast. These forms are present in a more dynamic beaches where cusps are often observed. In the southern part of the study area, a regular transverse bar system is also observed (Figure 8G). The two different types of bedform have been analyzed separately as they develop sub perpendicular to the shoreline or with a patchy distribution showing different sinuosity and length offshore the Outer Bar (OB; Figure 8H).

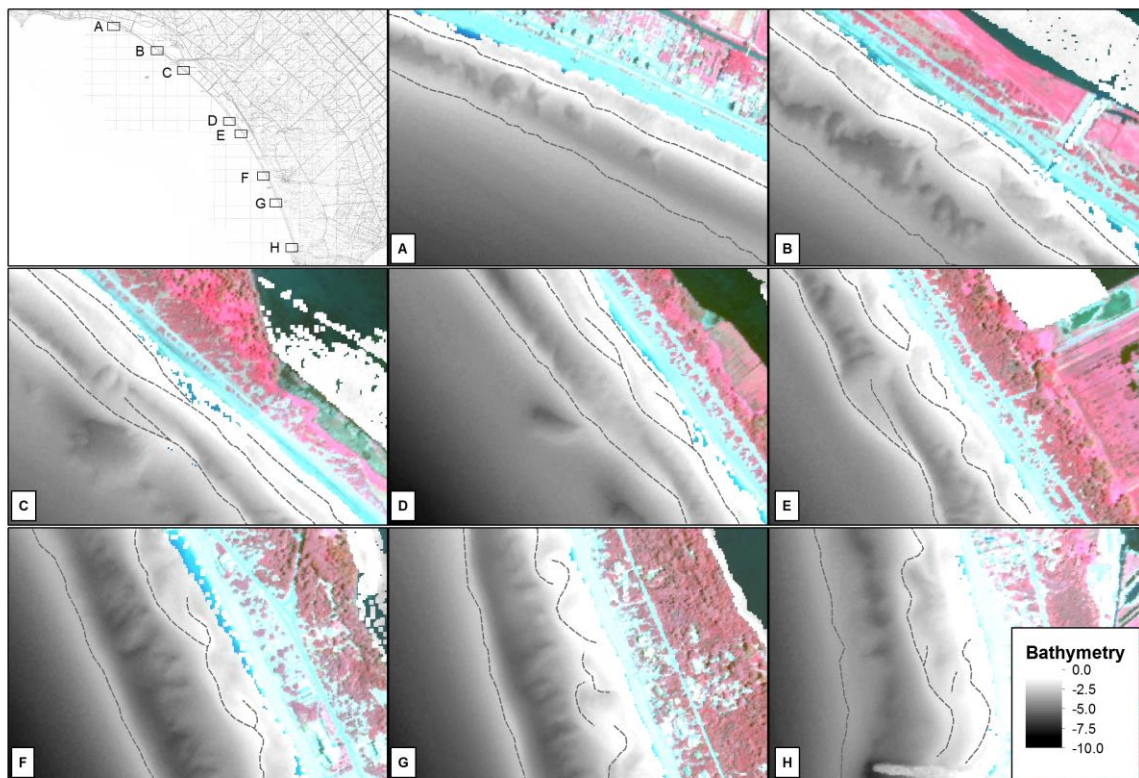


Figure 8. Bed-forms observed, moving in the southward direction. (A) LTT and OB; (B) LTT IB and OB; (C) example of bifurcation of the OB crest; (D) example of bifurcation of the inner bar; (E) sinusoid system of TBR; (F) bifurcated system of TBR and (G) regularly detached system of TBR (H) LTT sinusoid IB and regular OB. Submerged. Despite the different sinuosity two (A,D–G) or three (B–D,H) sand bars orders are observed along the studied shoreface.

With the obtained dataset some of the main parameters describing the characteristics of the submerged bars have been displayed. In particular, the characteristics along the first order sand bar has been analysed as it is the smaller in size, closer to the shoreline and the most sensitive to hydrodynamic regime. Crest depth, distance from the shoreline, and the length of the sandbar crest have been highlighted through simple dot diagrams.

The results show that the sector most affected by erosion is the one where the bar system present shorter crests. Here, sand bars are shorter because their sinuosity increases, and from continuous long-linear sand bars, they evolve in a wavy crest compared to the northern part of the study area

(Figure 9A,B). The correlation of distance from the shoreline and depth of the crest of each sand bar revealed the highest correlation coefficient for the middle features (those between the bars closer and farther from the emerged beach (Figure 9C). This trend explains the morphological evidence observed in the area, such as cusps along the shoreline discussed by [40,44].

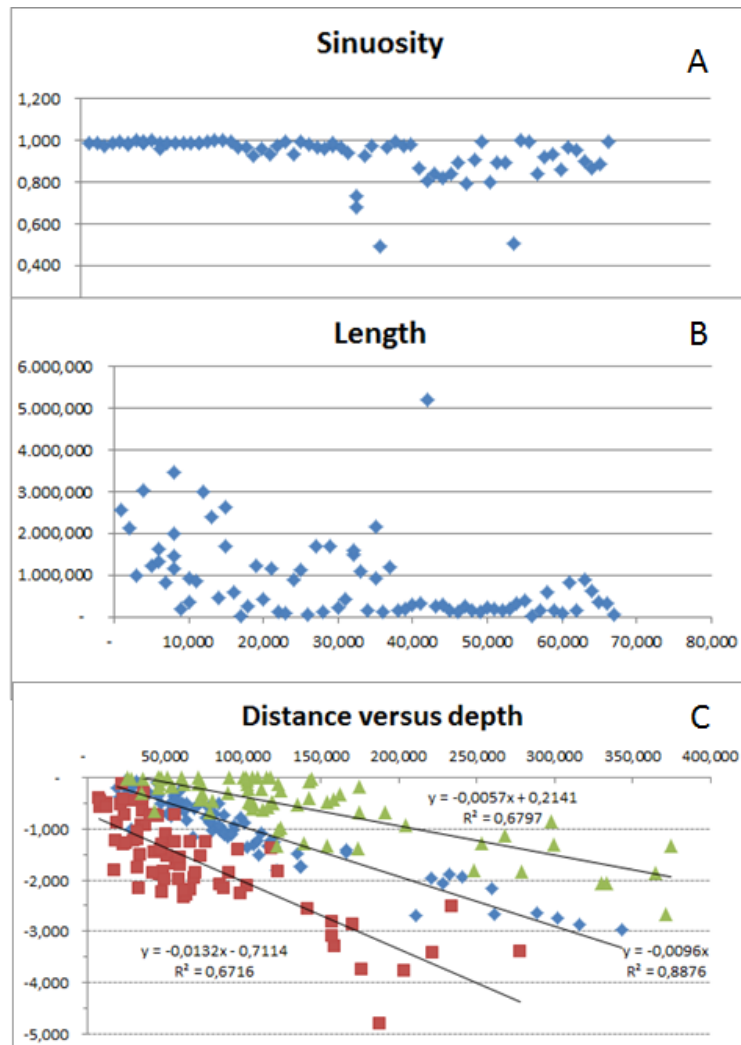


Figure 9. Sinuosity, length and distance versus depth of the sandbars system. (A,B) Sand bars from continuous long-linear sand bars evolve in a wavy crest moving southward; (C) correlation of distance versus depth of each sand bar's crest from the shoreline.

The present research, through the implementation of FHyl approach in submerged coastal environment, allowed to understand the morphology of the submerged beach within the study area. Sand bars are detached from the shoreline and increase their shape and sinuosity along the coastal stretch. The resulting bar system highlights the complex dynamic between the peculiar habitats and the observed morphological features. The littoral drift is from NW to SE, and some of the bars are close to the shoreline. They can occasionally transfer sand on the emerged beach creating cusped morphology [40,44]. Along the shoreline, there is an alternation of erosion and accretion phenomena. The presence of cusp is due to a typical rip-currents circulation, commonly associated with the presence of an asymmetric (and very undulating) bar system of the submerged beach.

The analysis of LiDAR data allows to observe the morphological evidence of sediment transport processes and thus to characterize the morphological variability of the beach-dune system. The most common morphologies of bar systems are Low Tide Terrace (LTT) and Transverse Bar and Rip (TBR) of

1° order (Inner Bar), 2° order (Intermediate or Outer Bar) and 3° order (Outer Bar; see for example box B, in Figure 10).

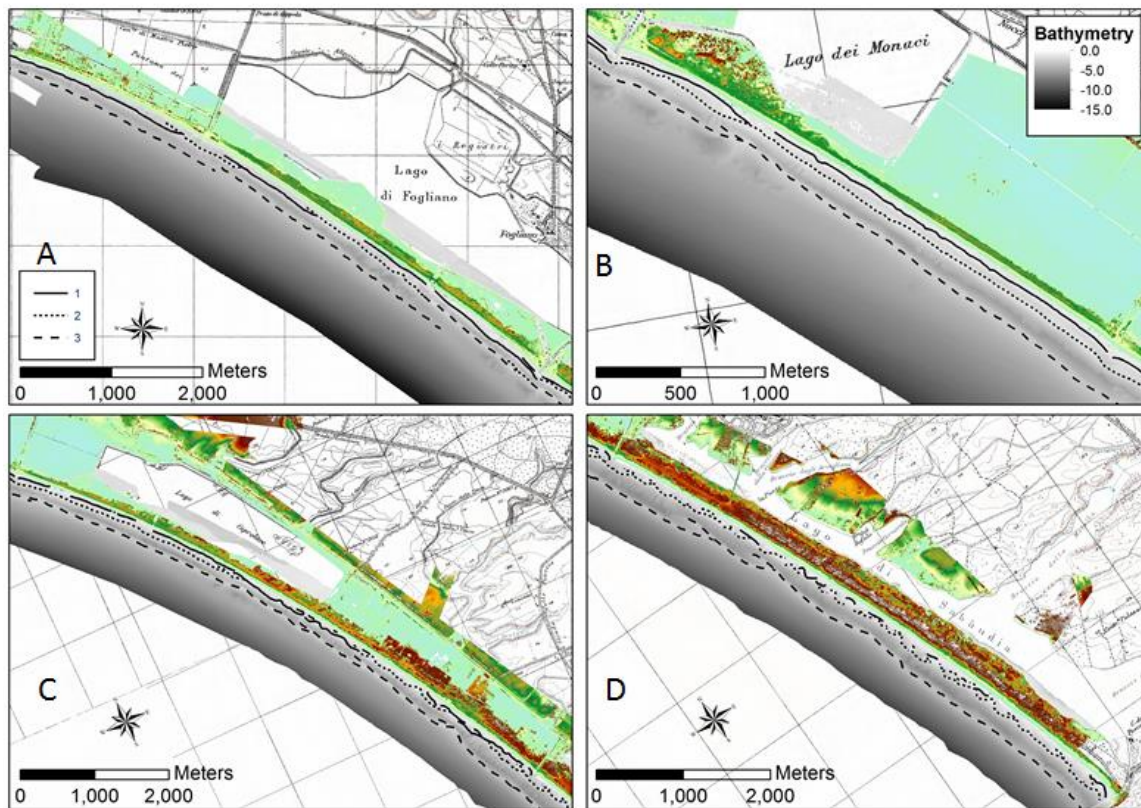


Figure 10. Examples of different morpho-bathymetric asset of sand bar crest (black lines) within the study area. From North to south the following bedforms can be observed: (A) IB and OB with some evidence of LTT in the southern part; (B) well developed and linear LTT, IB and OB system (C) Presence of the OB and passage from LTT and IB to TBR in the southern part; (D) fully developed TBR in the inner part of the submerged beach and in some part of the OB.

5. Discussion

The observation of the entire coastal stretch reveals the presence of a system of sandbars almost parallel to the coastline. This system tends to drift towards greater depths proceeding from N to S, until to reach, and cross the Rio Martino mouth near of 200 m from the shoreline. From the Lake of Sabaudia to Torre Paola, the behaviour of the sandbar system is different: the forms extend beyond 200 m and up to about 300 m from the shoreline with a wavy pattern especially evaluable for the outer bar (Figure 10).

Groynes realized to connect coastal lakes to the sea affect only partially the longshore transport [40,41,44] and seems to not interrupt the sandbar development. Some erosion and accumulation trends are evident nearby armed mouths of channels that connect coastal lakes to the sea (e.g., Fogliano, Monaci Caprolace, Sabaudia; see Figure 1), but the effect on the shoreface is limited to few meters. According to [44], the presence of the dunes, both natural and influenced by human structures, plays a key role in the size of shoreface bedforms and of their spatial variability and distribution.

Beyond the type of approach used for classification, it must be considered that bedforms represent the sediment response to the hydrodynamic forcing by acting to retard the wave energy flux over the seafloor. So, the main components to consider for a correct interpretation of processes and bedforms within a study area are the hydrodynamic regime and the nature of the seafloor on which the waves and currents exert their shear stress. For a more accurate assessment of the coastal system dominated by bedforms, it is important to consider the characteristics of the substrate, the presence of

bedrocks and the thickness of the sedimentary layer [71]. Shoreface slope, topo-bathymetry, as well as the nearshore and offshore sand bar positions (length, shape and distance from the shoreline) may influence incident waves propagation (direction, period, heights) and, consequently, the longshore currents. Consequently, the littoral drift can be influenced depending from the grain size of particles. All these factors affect the nature (number, size, type) of shoreface connected bed-forms and their evolution along the coastal stretch as discussed in literature [72]. A longshore bar system may follow a rhythmic arrangement lying classes of crescent/ic (or lunate) bar unit [40]. Several authors investigated how longshore bars represent a pulsating zone of active migration of sediments due to breaking waves and currents [2,44]. The high energy dissipative features are the Longshore Bar-Trough (LBT), then the Rhythmic Bar-Beach (RBB), the Transverse Bar and Rip (TBR) and finally the Low Tide Terrace (LTT), also known as 'ridge and runnel'. In the present study, the TBR revealed an asymmetry suggesting that their genesis and evolution is influenced both by rip currents and long-shore currents that allowed us to distinguish stoss and lee side (Figure 11).

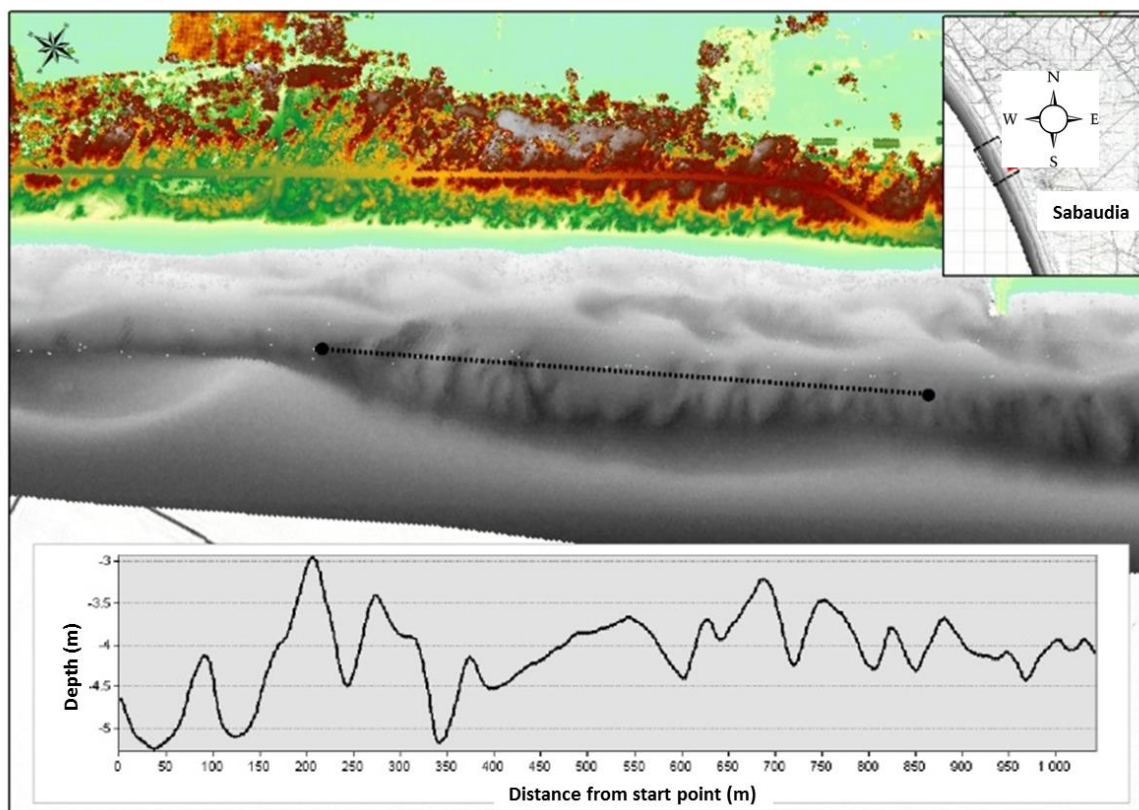


Figure 11. Detailed of the Outer bar (OB). A bathymetric profile (1000 m in length), parallel to the shoreline (black dotted line), demonstrates the asymmetry of the bed forms oriented perpendicular to the outer bar on the shoreface.

In the study area there is no presence of vegetation on the submerged beach. Some evidence of the *Posidonia oceanica* meadow was indicated about 10 km north but it has been subject to abrupt regression after the construction of the nuclear power station of Borgo Sabotino and the consequent release of warmer water from the reactor at about 2 km north from the studied area. So, the presence of vegetation (seagrass or algae) can be considered negligible for the aim of the present study. Nevertheless we cannot exclude that in some spot of the northern part the vegetation can affect the bedforms development and their southward migration.

Furthermore, for a more accurate assessment of the sediment response in nearshore barred system also the hydrodynamic forces acting on the seafloor should be considered.

5.1. Data Accuracy

The accuracy of raw data was carefully verified, comparing the differences observed between the bathymetric profiles measured with the LiDAR and the echo-sounder. We have taken into account that the algorithms of the airborne hydrography, used by Bloom Aereofilms for the final point cloud generation, calibrates the post-processing data by using a topographic RTK [73,74]. From literature [50], the specific LiDAR signal returns from different targets without considering the full waveforms, showing results of beam propagation in water, which expands in a different way after rebound/backscatter. The effective diameter in deep water is half the depth (number of scattering lengths), while in shallow water this causes an overestimation of the bathymetry ([24] with errors estimated up to 50 cm).

An overestimation of the depth could be related to the density of data acquisition, specifically to the number of points available within a single cell (in our case 4×4 m). Based on literature [40], the area ratio (equal to 1.78 for 3×3 m, to 0.64 for 5×5 m, and to 0.16 for 10×10 m) for the minimum cell detection provides a value correlated to the final accuracy.

Beside this general trend towards the overestimation of the bathymetric data-set by using LiDAR technology, we also notice (Figure 6c) that the accuracy of bathymetric data-set acquired in the surf zone (between 1 and 2.5 m of depth) by the use of the echo-sounder may be affected by the wave action in the surf zone [75–78] (where the waves are higher). It is commonly observed phenomena during bathymetric survey where above crest, reduction of water depth increases the incident waves height, even during calm conditions. More interesting is the increase of differences between LiDAR and Echo sounder dataset off shore at more than 7.5 m of depth. This value curiously matches with the closure depth [1,6,9].

5.2. Data Analysis and Elaboration Techniques

Seafloor characterization is an important issue that has been recently discussed by [75], considering the possibility of auto classification, as well as cognitive interpretation of digital bathymetric data, in terms of geomorphological features [74,79,80].

The world of mapping and data visualization is quickly evolving into a three and four dimensional context, and the utility of LiDAR technology have been proven in a variety of scientific communities [80,81]. However, the challenge is to expand LiDAR awareness among non-technical audiences considering the high complexity of coastal areas and others who need information solutions that LiDAR can support. Within this study, light detection and ranging (LiDAR) shows how both of them are suitable for mapping coastal shallow waters, beach profiles and concentrations of suspended particles in coastal waters. Since coastal ecosystems have high spatial complexity and temporal variability, they should be observed with high spatial, spectral, and temporal resolutions. Combining these techniques and using time-series of images enables scientists to study the coastal ecosystems and accurately determine long-term trends and short-term changes [82].

5.3. Use of Remote Sensing Products for Coastal Management

Our dataset and paper highlight challenges and opportunities that recent advances in remote sensing offer for accurate physical mapping. The dissemination activities that supported the development of this research are extremely relevant as for the first time ever stakeholders and competent authorities could see the morphology of sand bar system and better understand where and how to plan beach erosion intervention in correlation to public needs. Based on the elaborations of the present paper, and also thanks to the capability to “classify” and map (3D) the submerged sand bar system, stakeholders and competent Authorities have decided to use the results of the present study to perform coastal erosion mitigation actions.

An experimental intervention is going to be carried out on May 2020 in the study area. The project foresees the enlargement of about 2000 m the emerged beach during the tourist season to increase the

carrying capacity and the receptivity of the coast [83]. About 20,000 m³ of sand will be dredged from the shoreface between the crest and the slope of the inner bar (IB) and spill over the trough between the crest of the inner bar (IB) and the shoreline (Figure 12).

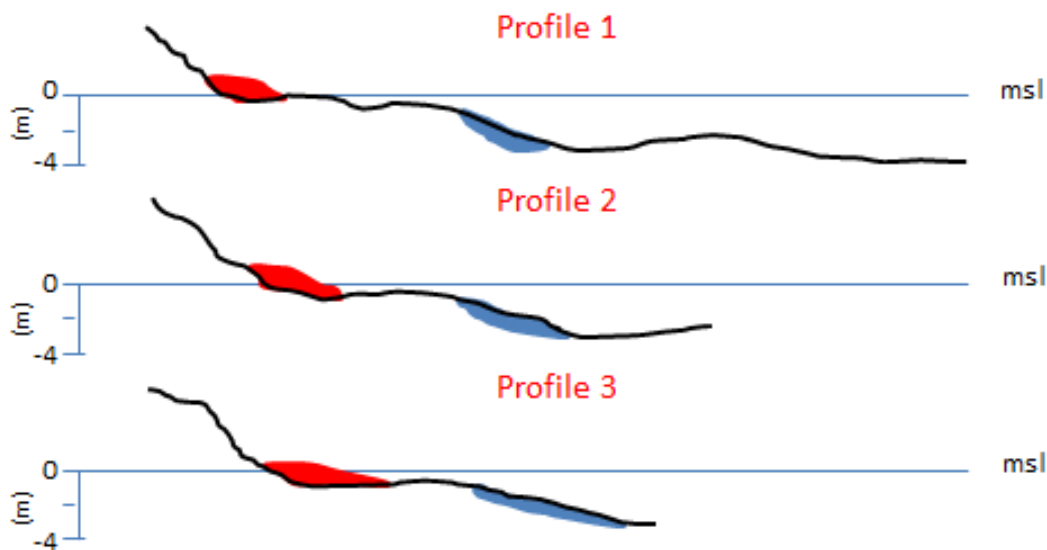


Figure 12. A simplified sketch of the dredging area (blue) and nourishment area (red) are reported along three profiles of the beach-dune system (black line) in front of Fogliano Lake (norther part of the studied area more exposed to erosion and tourists).

5.4. Cost of Remote Sensing Survey and Contribute of FHyl to National RS Plan

Considering the strong interest that science for environmental policy has recently gained in the European context we have made an effort to calculate the final costs of this approach:

- | | |
|---------------------------------------|---|
| 1. Airborne multisensory acquisition: | ~ 1600 €/km ² (for about 100 km ²) 160,000 € |
| 2. Field data analysis: | ~ 5000 € (see also Valentini et al., 2020, this SI) |
| 3. Logistic and surveys: | ~ 300 €/km ² (fieldwork and dissemination) |
| 4. Processing was 1:1 (man month): | ~ 1500 €/km ² (for about 100 km ²) 150,000 € |
| 5. Post processing 1/3: | ~ 530 €/km ² (software, workstation, etc . . .) |

These costs (~345,000 € for about 100 km²) can be considered proportional to the resolution (Figure 13).

Costs are diminishing across a temporal scale. In this monitoring study, the first in Italy in its own characteristics (LIDAR and MIVIS), the highest effort has certainly been processing and post processing [82]. The reason is that procedures for coastal integrated analysis were not implemented and the ground truth protocol required with new remote sensing technologies was not adequate. With the present work and the overall results of the research, standards for data and processing tools have been developed contributing to a reduction of processing and post processing effort (i.e., cost of RS survey and products). Following contract conducted by the authors demonstrated a rapid and significant decrease of the cost [84], a reduction of time to obtain higher quality elaborations and higher resolution maps. The need for periodic beach nourishment involves periodic topo-bathymetric surveys of the coast. The FHyl methodology can certainly influence the cost-effectiveness of the surveys both in terms of time and cost reduction through time. The research developed a benchmark under the framework of different area acquisition for The National LiDAR Map implementation, which requires multiple datasets that are seamless and nationwide. The National LiDAR Dataset (part of the Italian Remote Sensing National Plan) has already been demonstrated to provide structures and vegetative cover as well as topography in a single time frame in coastal and fluvial areas [31,85–87].

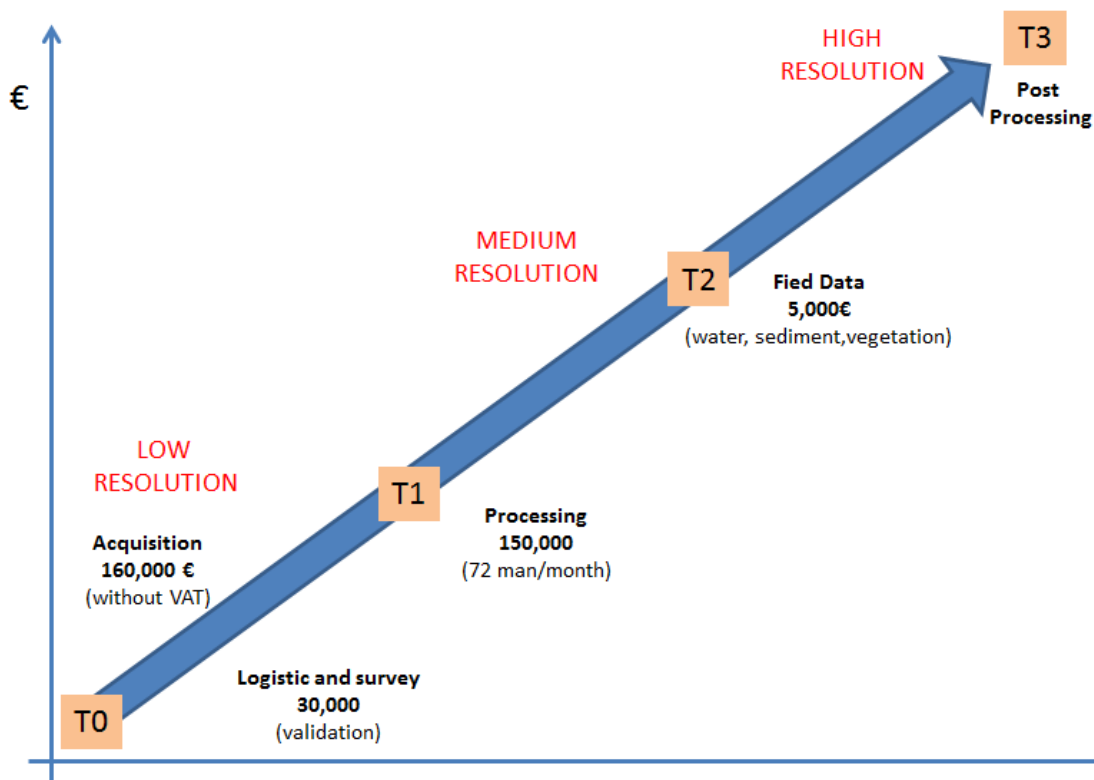


Figure 13. Visual representation of costs in relation to the resolution of obtained results.

6. Conclusions

The Sabaudia coastal area is a highly valued environment where different habitats interact with morphological features, determining a complex state of dynamic equilibrium. The study of the coastal morphology through innovative techniques implemented remotely represent a new systematic approach named FHyl (field spectral libraries, airborne hyperspectral images and topographic LiDAR) for acquisition and processing of LiDAR data for the quantitative assessment of different morphological features characterizing the bottom surface. The new approach shows the impressive results of physical characterization based on the use of the LiDAR remote sensing data. The use of LiDAR offered the chance to explore vast areas, by providing high quality information related the geometry (morphotypes) and the dynamics of sand bars.

In particular, the LiDAR parameters obtained in this study allowed to the identification of the position and the sinuosity of nearshore bars also referring to the shoreline position.

The obtained products give information on the sub-merged morphological parameters and provide a first attempt to identify their complex variability in time and space. Large scale bedform analysis, that allows to recognize complex conceptual models of landform and to reveal evidence of evolutionary processes, is out of the scope of this work as it is still under investigation by the authors. The obtained results have enabled to produce synthetic maps describing the key morphological parameters (e.g., slope and direction of bed-forms, water depth) in the nearshore zone (e.g., sandbar migration and their effects on shoreline evolution) related to the coastal dynamic. These products have influenced the local authorities and stakeholders who, for the first time, adopted a beach nourishment strategy based on the sand transfer along the beach profile. Bedforms represent the sediment response to the hydrodynamic forcing by acting to retard the wave energy flux over the seafloor. Their periodic survey and morphological response to dredging operations in very shallow water surely encourages the periodic acquisition of remote sensing data for supporting marine scientists and stakeholders to better understand the complex morphological processes affecting the coastal evolution, thus leading to more effective management of the beach erosion control.

The methodology for coastal mapping described in the present work also aims to bridge the existing gaps between the scientific community and users, as well as research products and operators of the sector.

Author Contributions: Conceptualization, S.C., and A.T.; methodology, L.R., E.V., S.C.; formal analysis, L.R., E.V., S.C., I.L.; resources, E.V. and A.T.; data curation L.R., S.C., E.V., I.L.; all authors contributed to write, review and edit the original manuscript; visualization, L.R.; supervision, A.T. and S.C.; project administration, A.T.; funding acquisition, A.T. The corresponding author S.C. and the co-author E.V. are the contacts to access the dataset. All authors have read and agreed to the published version of the manuscript.

Funding: This research has been funded by the Lazio Region within the CAMP Project (2009) and the publication of this manuscript is supported and exploited by the ISPRA agreement with the Italian Space Agency for the ‘Habitat Mapping’ (Agreement number A0HMASI2).

Acknowledgments: Special thanks is addressed to Eng. Paolo Lupino for his interest and support. Thanks to the firm BLOOM-CGR for the logistics and execution of the LiDAR/MIVIS hyperspectral airborne campaign. Thanks to Carlo Innocenti, Matteo Conti, Alfredo Pazzini, Raffaele Proietti for the ground-truthing campaign and to Irene Mammi for the pre-elaboration; to Coastal Regeneration Maintenance spiagge srl, (CO.RE.MA.) for sharing the updated information of the ongoing beach protection project (Figure 11).

Conflicts of Interest: The authors declare no conflict of interest.

References

- Short, A.D. *Handbook of Beach and Shoreface Morphodynamics*; Wiley: West Sussex, UK, 1999; p. 379.
- Armaroli, C.; Grotoli, E.; Harley, M.D.; Ciavola, P. Beach morphodynamics and types of foredune erosion generated by storms along the Emilia-Romagna coastline, Italy. *Geomorphology* **2013**, *199*, 22–35. [[CrossRef](#)]
- Stive, M.J.F.; Aarninkhof, S.G.J.; Hamm, L.; Hanson, H.; Larson, M.; Wijnberg, K.M.; Nicholls, R.J.; Capobianco, M. Variability of shore and shoreline evolution. *Coast. Eng.* **2002**, *47*, 211–235.
- Benedet, L.; Finkl, C.W.; Campbell, T.; Kleing, A. Predicting the effect of beach nourishment and cross-shore sediment variation on beach morphodynamic assessment. *Coast. Eng.* **2004**, *51*, 839–861. [[CrossRef](#)]
- Kraus, N.C.; Larson, M.; Kriebel, D.L. Evaluation of beach erosion and accretion predictors. *Proc. Coast. Sediments Conf. (SeattleAsce)* **1991**, *1*, 572–587.
- Van Rijn, L.C. *Principles of Coastal Morphology*; Aqua Publications: Blokzijl, The Netherlands, 1998; p. 730.
- Lipman, T.C.; Holman, R.A. The spatial and temporal variability of sand bar morphology. *J. Geophys. Res.* **1990**, *95*, 1575–1590. [[CrossRef](#)]
- Klein, A.H.F.; Menezes, J.T. Beach morphodynamics and profile sequence for headland bay coast. *J. Coast. Res.* **2001**, *17*, 812–835.
- Lisi, I.; Molfetta, M.G.; Bruno, M.F.; Di Risio, M.; Damiani, L. Morphodynamic classification of sandy beaches in enclosed basins: The case study of Alimini (Italy). *J. Coast. Res.* **2011**, *SI 64*, 180–184.
- Traganos, D.; Poursanidis, D.; Aggarwal, B.; Chrysoulakis, N.; Reinartz, P. Estimating satellite-derived bathymetry (SDB) with the google earth engine and sentinel-2. *Remote Sens.* **2018**, *10*, 859. [[CrossRef](#)]
- Misra, A.; Vojinovic, Z.; Ramakrishnan, B.; Luijendijk, A.; Ranasinghe, R. Shallow water bathymetry mapping using Support Vector Machine (SVM) technique and multispectral imagery. *Int. J. Remote Sens.* **2018**, *39*, 4431–4450. [[CrossRef](#)]
- Kasvi, E.; Salmela, J.; Lotsari, E.; Kumpula, T.; Lane, S.N. Comparison of remote sensing based approaches for mapping bathymetry of shallow, clear water rivers. *Geomorphology* **2019**, *333*, 180–197. [[CrossRef](#)]
- Agrafiotis, P.; Karantzas, K.; Georgopoulos, A.; Skarlatos, D. Correcting image refraction: Towards accurate aerial image-based bathymetry mapping in shallow waters. *Remote Sens.* **2020**, *12*, 322. [[CrossRef](#)]
- Dietrich, J.T. Bathymetric structure from motion: Extracting shallow stream bathymetry from multi view stereo photogrammetry. *Earth Surf. Process. Landf.* **2017**, *42*, 355–364. [[CrossRef](#)]
- Guenther, G.C. Airborne Lidar bathymetry. In *Digital Elevation Model Technologies and Applications: The DEM Users Manual*; American Society of Photogrammetry and Remote Sensing: Bethesda, MD, USA, 2007; pp. 253–320.
- Deronde, B.; Houthuys, R.; Debruyne, W.; Franssaer, D.; Lancker, V.V.; Henriët, J.-P. Use of airborne hyperspectral data and laserscan data to study beach morphodynamics along the Belgian coast. *J. Coast. Res.* **2006**, *225*, 1108–1117. [[CrossRef](#)]

17. Schwarz, R.; Mandlbauer, G.; Pfennigbauer, M.; Pfeifer, N. Design and evaluation of a full-wave surface and bottom-detection algorithm for LiDAR bathymetry of very shallow waters. *ISPRS J. Photogramm. Remote Sens.* **2019**, *150*, 1–10. [[CrossRef](#)]
18. Kogut, T.; Bakula, K. Improvement of full waveform airborne laser bathymetry data processing based on waves of neighborhood points. *Geosciences* **2019**, *11*, 1255. [[CrossRef](#)]
19. Manzo, C.; Valentini, E.; Taramelli, A.; Filipponi, F.; Disperati, L. Spectral characterization of coastal sediments using field spectral libraries, airborne hyperspectral images and topographic LiDAR data (FHyL). *Int. J. Appl. Earth Obs. Geoinf.* **2015**, *36*, 54–68. [[CrossRef](#)]
20. Adam, S.; De Backer, A.; De Wever, A.; Sabbe, K.; Tooman, E.A.; Vinex, M.; Monbaliu, J. Bio-physical characterization of sediment stability in mudflat using remote sensing: A laboratory experiment. *Cont. Shelf Res.* **2011**, *31* (Suppl. S10), S26–S35. [[CrossRef](#)]
21. Athearn, N.D.; Takekawa, J.Y.; Jaffe, B.; Hattenbach, B.J.; Foxgrover, A.C. Mapping elevations of tidal wetland restoration sites in San Francisco Bay: Comparing accuracy of aerial LiDAR with a singlebeam echosounder. *J. Coast. Res.* **2010**, *26*, 312–319. [[CrossRef](#)]
22. Brock, J.C.; Purkis, M.J. The emerging role of LiDAR remote sensing in coastal research and resource management. *J. Coast. Res.* **2009**, *53*, 1–5. [[CrossRef](#)]
23. Davidson-Arnott, R.G.D. Conceptual model of the effects of sea level rise on sandy coasts. *J. Coast. Res.* **2005**, *26*, 1166–1172. [[CrossRef](#)]
24. Goodman, J.A.; Lee, Z.P.; Ustin, S.L. Influence of atmospheric and sea-surface corrections on retrieval of bottom depth and reflectance using a semi-analytical model: A case study in Kaneohe Bay, Hawaii. *Appl. Opt.* **2008**, *47*, F1–F11. [[CrossRef](#)] [[PubMed](#)]
25. Malthus, T.J.; Mumby, P.J. Remote sensing of the coastal zone: An overview and priorities for future research. *Int. J. Remote Sens.* **2003**, *24*, 2805–2815. [[CrossRef](#)]
26. Taramelli, A.; Valentini, E.; Cornacchia, L.; Bozzeda, F. A hybrid power law approach for spatial and temporal pattern analysis of salt marsh evolution. *J. Coast. Res.* **2017**, *77* (Suppl. S1), 62–72. [[CrossRef](#)]
27. Töyrä, J.; Pietroniro, A. Towards operational monitoring of a northern wetland using geomatics-based techniques. *Remote Sens. Environ.* **2005**, *97*, 174–191. [[CrossRef](#)]
28. Prasad, A.D.; Jain, K.; Gairola, A. Mapping of lineaments and knowledge base preparation using geomatics techniques for part of the Godavari and Tapi basins, India: A case study. *Int. J. Comput. Appl.* **2013**, *70*, 39–47.
29. Ajmar, A.; Boccardo, P.; Disabato, F. Rapid Mapping: Geomatics role and research opportunities. *Rend. Fis. Acc. Lincei.* **2015**, *26*, 63–73. [[CrossRef](#)]
30. Valentini, E.; Taramelli, A.; Filipponi, F.; Giulio, S. An effective procedure for EUNIS and Natura 2000 habitat type mapping in estuarine ecosystems integrating ecological knowledge and remote sensing analysis. *Ocean Coast. Manag.* **2015**, *108*, 52–64. [[CrossRef](#)]
31. Cappucci, S.; Valentini, E.; Monte, M.D.; Paci, M.; Filipponi, F.; Taramelli, A. Detection of natural and anthropic features on small islands. *J. Coast. Res.* **2017**, *77* (Suppl. S1), 73–87. [[CrossRef](#)]
32. Bellucci, G.; Altieri, F.; Bibring, J.P.; Bonello, G.; Langevin, Y.; Gondet, B.; Poulet, F. OMEGA/Mars Express: Visual channel performances and data reduction techniques. *Planet. Space Sci.* **2006**, *54*, 675–684. [[CrossRef](#)]
33. Barducci, A.; Guzzi, D.; Marcoionni, P.; Pippi, I. Aerospace wetland monitoring by hyperspectral imaging sensors: A case study in the coastal zone of San Rossore Natural Park. *J. Environ. Manag.* **2009**, *90*, 2278–2286. [[CrossRef](#)]
34. Boschetti, M.; Boschetti, L.; Oliveri, S.; Casati, L.; Canova, I. Tree species mapping with Airborne hyper-spectral MIVIS data: The Ticino Park study case. *Int. J. Remote Sens.* **2007**, *28*, 1251–1261. [[CrossRef](#)]
35. Calvo, S.; Ciruolo, G.; La Loggia, G. Monitoring *Posidonia oceanica* meadows in a Mediterranean coastal lagoon (Stagnone, Italy) by means of neural network and ISODATA classification methods. *Int. J. Remote Sens.* **2003**, *24*, 2703–2716. [[CrossRef](#)]
36. Giardino, C.; Brando, V.E.; Dekker, A.G.; Strömbeck, N.; Candiani, G. Assessment of water quality in Lake Garda (Italy) using Hyperion. *Remote Sens. Environ.* **2007**, *109*, 183–195. [[CrossRef](#)]
37. Marani, M.; Belluco, E.; Ferrari, S.; Silvestri, S.; D’Alpaos, A.; Lanzoni, S.; Feola, A.; Rinaldo, A. Analysis, synthesis and modelling of high-resolution observations of salt-marsh ecogeomorphological patterns in the Venice lagoon. *Estuar. Coast. Shelf Sci.* **2006**, *69*, 414–426. [[CrossRef](#)]

38. Marani, M.; Silvestri, S.; Belluco, E.; Ursino, N.; Comerlati, A.; Tosatto, O.; Putti, M. Spatial organization and ecohydrological interactions in oxygen-limited vegetation ecosystems. *Water Resour. Res.* **2006**, *42*, W06D06. [CrossRef]
39. Lazio Region. Monitoring Centre of Integrated Coastal Zone Management. 2020. Available online: http://www.cmgizc.info/index.php?option=com_content&view=category&id=24&Itemid=184&lang=it (accessed on 1 January 2020).
40. Pallottini, E.; Cappucci, S.; Taramelli, A.; Innocenti, C.; Screpanti, A. Variazioni morfologiche stagionali del sistema spiaggia-duna del Parco Nazionale del Circeo. *Studi Costieri* **2010**, *17*, 105–124.
41. Campo, V.; La Monica, G.B. Le dune costiere oloceniche prossimali lungo il litorale del Lazio. *Studi Costieri* **2006**, *11*, 31–42.
42. Blanc, A.C.; Segre, A. Le auatenaire du monte circeo. Livret guide. In Proceedings of the IV Congrès INQUA, Rome, Italy; 1953, pp. 23–108. Available online: <https://www.google.com.hk/url?sa=t&rct=j&q=&esrc=s&source=web&cd=3&ved=2ahUKEwilnryV4bfoAhVU7WEKHWjCCAIQFjACegQIBhAB&url=https%3A%2F%2Fbooks.google.com%2Fbooks%2Fabout%2FINQUA.html%3Fid%3Dnv7nM2CWO4sC&usq=AOvVaw1H7uWKDdmQmv9rr3Ofxv6K> (accessed on 14 February 2020).
43. Giovagnotti, C.; Rondelli, F.; Pascoletti, F.T. Caratteristiche geomorfologiche e sedimentologiche delle formazioni quaternarie del litorale laziale tra T.re Astura e il M. Circeo. *Estratto Degli Annu. Della Fac. Agrar. Dell'università Perugia* **1980**, *34*, 173–235.
44. Pallottini, E.; Cappucci, S. Beach—Dune system interaction and evolution. *Rend. Online Soc. Geol. Ital.* **2009**, *8*, 87–97.
45. Koppari, K.; Karlsson, U.; Steinvall, O. Airborne laser depth sounding in Sweden. International hydrographic review. *Monaco* **1994**, *71*, 69–90.
46. Schnurr, D. High speed Hawk Eye delivers new efficiencies in coastal zone mapping. *Port Eng. Manag.* **2009**, *27*, 2.
47. Guenther, G.C.; LaRocque, P.E.; Lillycrop, W.J. Multiple surface channels in Scanning Hydrographic Operational Airborne LiDAR Survey (SHOALS) airborne LiDAR. In Proceedings of the Ocean Optics XII, Bergen, Norway, 13–15 June 1994; pp. 422–430.
48. Thomas, R.W.L.; Guenther, G.C. Water surface detection strategy for an airborne laser bathymeter. In Proceedings of the Ocean Optics X, Orlando, FL, USA, 1 September 1990; p. 597.
49. Guenther, G.C. Wind and nadir angle effects on airborne LiDAR water'surface' returns. In Proceedings of the Ocean optics VIII, Orlando, FL, USA, 31 March–2 April 1986; pp. 277–286.
50. Guenther, G.C.; Thomas, R.W.L. *Prediction and Correction of Propagation-induced Depth Measurement Biases Plus Signal Attenuation and Beam Spreading for Airborne Laser Hydrography*; NOAA Technical Report NOS: Rockville, MD, USA, 1984. Available online: http://www.ngs.noaa.gov/PUBS_LIB/PredictionAndCorrectionOfPropagationInducedDepthMeasurementBiasesForAirborneLaserHydrography_TR_NOS106_CGS2.pdf (accessed on 19 March 2020).
51. ISPRA. *Rilievo di Dettaglio Della Batimetria Costiera Laziale con Tecnologie Lidar e Valutazione Delle Caratteristiche Fisiche e Biologiche in Aree Marine Della Costa Laziale di Specifico Interesse Ambientale Fase 2-Caratterizzazione Morfologica*; ISPRA: Rome, Italy, 2009; 120p.
52. Available online: <http://www.caris.com/products/hips-sips/> (accessed on 14 February 2020).
53. Available online: <http://woodshole.er.usgs.gov/project-pages/dsas/> (accessed on 14 February 2020).
54. Available online: http://www.cmgizc.info/index.php?option=com_content&view=article&id=33:lidar-convenzione-ispra&catid=24&Itemid=184&lang=it (accessed on 14 February 2020).
55. Taramelli, A.; Valentini, E.; Innocenti, C.; Cappucci, S. FHyl: Field spectral libraries, airborne hyperspectral images and topographic and bathymetric LiDAR data for complex coastal mapping. In Proceedings of the 2013 IEEE International Geoscience and Remote Sensing Symposium-IGARSS, Melbourne, Australia, 21–26 July 2013; pp. 2270–2273.
56. Irish, J.L.; White, T.E. Coastal engineering applications of high-resolution LiDAR bathymetry. *Coast. Eng.* **1998**, *35*, 47–71. [CrossRef]
57. Quadros, N.D.; Collier, P.A.; Fraser, C.S. Integration of bathymetric and topographic LiDAR: A preliminary investigation. *Int. Arch. Photogramm. Remote Sens. Spat. Inf. Sci.* **2008**, *37*, 1299–1304.
58. Shepard, F.P. Beach cycles in southern California. In *Technical Memorandum*; Beach Erosion Board, US Army Corps of Engineers: Washington, DC, USA, 1950; Volume 20, p. 31.

59. Verfaillie, E.; Van Lancker, V.; Van Meirvenne, M. Multivariate geostatistics for the predictive modelling of the surficial sand distribution in shelf seas. *Cont. Shelf Res.* **2006**, *26*, 2454–2468. [[CrossRef](#)]
60. Lucieer, V.L. *Spatial Uncertainty Estimation Techniques for Shallow Coastal Seabed Mapping*; University of Tasmania: Hobart, Australia, 2007; Available online: <http://eprints.utas.edu.au/1919/> (accessed on 19 March 2020).
61. Micallef, A.; Le Bas, T.P.; Huvenne, V.A.I.; Blondel, P.; Huhnerbach, V.; Deidun, A. A multi-method approach for benthic habitat mapping of shallow coastal areas with high-resolution multibeam data. *Cont. Shelf Res.* **2012**, *39–40*, 14–26. [[CrossRef](#)]
62. Diesing, M.; Thorsnes, T. Mapping of cold-water coral carbonate mounds based on geomorphometric features: An object-based approach. *Geosciences* **2018**, *8*, 34. [[CrossRef](#)]
63. Janowski, L.; Trzcinska, K.; Tegowski, J.; Kruss, A.; Rucinska-Zjadacz, M.; Pocwiardowski, P. Nearshore benthic habitat mapping based on multi-frequency, multibeam echosounder data using a combined object-based approach: A case study from the Rowy site in the southern Baltic sea. *Remote Sens.* **2018**, *10*, 1983. [[CrossRef](#)]
64. Fogarin, S.; Madricardo, F.; Zaggia, L.; Sigovini, M.; Montereale-Gavazzi, G.; Kruss, A.; Lorenzetti, G.; Manfé, G.; Petruzzo, A.; Molinaroli, E.; et al. Tidal inlets in the Anthropocene: Geomorphology and benthic habitats of the Chioggia inlet, Venice Lagoon (Italy). *Earth Surf. Process. Landf.* **2019**, *44*, 2297–2315. [[CrossRef](#)]
65. Toso, C.; Madricardo, F.; Molinaroli, E.; Fogarin, S.; Kruss, A.; Petruzzo, A.; Pizzeghello, N.M.; Sinapi, L.; Trincardi, F. Tidal inlet seafloor changes induced by recently built hard structures. *PLoS ONE* **2009**, *14*, 29. [[CrossRef](#)]
66. Misiuk, B.; Diesing, M.; Aitken, A.; Brown, C.J.; Edinger, E.N.; Bell, T. A Spatially Explicit Comparison of quantitative and categorical modelling approaches for mapping seabed sediments using random forest. *Geosciences* **2019**, *9*, 254. [[CrossRef](#)]
67. Wilson, M.F.J.; O’Connell, B.C.; Brown, J.C.; Guinan, E.; Grehan, A.J. Multiscale terrain analysis of multibeam bathymetry data for habitat mapping on the continental slope. *Mar. Geod.* **2007**, *30*, 3–35. [[CrossRef](#)]
68. Sorichetta, A.; Seeber, L.; Taramelli, A.; McHugh, C.; Cormier, M. Geomorphic evidence for tilting at a continental transform: The Karamursel Basin along the North Anatolian Fault, Turkey. *Geomorphology* **2010**, *119*, 221–231. [[CrossRef](#)]
69. Taramelli, A.; Valentini, E.; Cornacchia, L.; Monbaliu, J.; Sabbe, K. Indications of dynamic effects on scaling relationships between channel sinuosity and vegetation patch size across a salt marsh platform. *J. Geophys. Res. Earth Surf.* **2018**, *123*, 2714–2731. [[CrossRef](#)]
70. Conti, M.; Cappucci, S.; La Monica, G.B. Sediment dynamic of nourished sandy beaches. *Rend. Line Soc. Geol. Ital.* **2009**, *8*, 31–38.
71. Ausili, A.; Cappucci, S.; Gabellini, M.; Innocenti, C.; Maffucci, M.; Romano, E.; Rossi, L.; Taramelli, A. New approaches for multi source data sediment characterisation, thickness assessment and clean up strategies. *Chem. Eng. Trans.* **2012**, *28*, 223–228.
72. Komar, P.D. *Beach Processes and Sedimentation*; Prentice-Hall: Englewood Cliff, NJ, USA, 1998; p. 429.
73. Isaksson, A. *Coastal Survey Studio Mark II Manual Version 2.X*; Airborne Hydrography AB: Jönköping, Sweden, 2009.
74. Schnurr, D. How low can you go? Maximum depth achieved with Hawk Eye II during project in 2009. In Proceedings of the International LiDAR mapping forum, Denver, CO, USA, 3–5 March 2010.
75. Finkl, C.W.; Makowski, C. Autoclassification versus cognitive interpretation of digital bathymetric data in terms of geomorphological features for seafloor characterization. *J. Coast. Res.* **2015**, *31*, 1–16. [[CrossRef](#)]
76. Yeu, Y.; Yee, J.J.; Yun, H.S.; Kim, K.B. Evaluation of the accuracy of bathymetry on the nearshore coastlines of western Korea from satellite altimetry, multi-beam, and airborne bathymetric LiDAR. *Sensors* **2018**, *18*, 2926. [[CrossRef](#)]
77. Costa, B.; Battista, T.A.; Pittman, S.J. Comparative evaluation of airborne LiDAR and ship-based multibeam SoNAR bathymetry and intensity for mapping coral reef ecosystems. *Remote Sens. Environ.* **2009**, *113*, 1082–1100. [[CrossRef](#)]
78. Pike, S.; Traganos, D.; Poursanidis, D.; Williams, J.; Medcalf, K.; Reinartz, P.; Chrysoulakis, N. Leveraging commercial high-resolution multispectral satellite and multibeam sonar data to estimate bathymetry: The case study of the Caribbean Sea. *Remote Sens.* **2019**, *11*, 1830. [[CrossRef](#)]

79. Tan, T.W.; Godin, O.A.; Brown, M.G.; Zobotin, N.A. Characterizing the seabed in the Straits of Florida by using acoustic noise interferometry and time warping. *J. Acoust. Soc. Am.* **2019**, *146*, 2321–2334. [[CrossRef](#)]
80. Masetti, G.; Faulkes, T.; Calder, B.R. Opening the black boxes in ocean mapping: Design and implementation of the hydroffice framework. Proceeding of the Australian Marine Sciences Association (Freemantle, AMSA), Perth, Australia, 7–11 July 2019. [[CrossRef](#)]
81. Stoker, J.; Harding, D.; Parrish, J. The need for a National LiDAR Dataset. *Photogramm. Eng. Remote Sens.* **2008**, *74*, 1066–1068.
82. White, S.A.; Parrish, C.E.; Calder, B.R.; Pe’eri, S.; Rzhanov, Y. LiDAR-derived national shoreline: Empirical and stochastic uncertainty analysis. *J. Coast. Res.* **2011**, *2011*, 62–74. [[CrossRef](#)]
83. Klemas, V. Remote sensing of emergent and submerged wetlands: An overview. *Int. J. Remote Sens.* **2013**, *34*, 6286–6320. [[CrossRef](#)]
84. Cappucci, S.; De Cecco, L.; Geremei, F.; Giordano, L.; Moretti, L.; Peloso, A.; Pollino, M. Earthquake’s rubble heaps volume evaluation: Expeditious approach through earth observation and geomatics techniques. *Lect. Notes Comput. Sci.* **2017**, *10405*, 261–277.
85. Cappucci, S.; Vaccari, M.; Falconi, M.; Tudor, T. The sustainable management of sedimentary resources. “The case study of Egadi Project”. *Environ. Eng. Manag. J.* **2019**, *18*, 317–328.
86. Pascucci, V.; Cappucci, S.; Andreucci, S.; Donda, F. Sedimentary features of the offshore part of the la Pelosa Beach (Sardinia, Italy). *Rend. Line Soc. Geol. Ital.* **2008**, *2*, 1–3.
87. Giardino, C.; Bresciani, M.; Valentini, E.; Gasperini, L.; Bolpagni, R.; Brando, V.E. Airborne hyperspectral data to assess suspended particulate matter and aquatic vegetation in a shallow and turbid lake. *Remote Sens. Environ.* **2015**, *157*, 48–57. [[CrossRef](#)]



© 2020 by the authors. Licensee MDPI, Basel, Switzerland. This article is an open access article distributed under the terms and conditions of the Creative Commons Attribution (CC BY) license (<http://creativecommons.org/licenses/by/4.0/>).